Arabian Journal for Science and Engineering (2021) 46:5633–5643
https://doi.org/10.1007/s13369-020-05166-2

RESEARCH ARTICLE-CHEMISTRY

Microstructure, Magnetic and Mössbauer Studies of Mechanically Alloyed FeCoNi Nanocrystalline Powders

Rakia Daly[1] · Nawel Khitouni[1,2] · Maria Luisa Escoda[2] · Núria Llorca Isern[3] · Sunol Martinez Juan Jose[2] · Jean Marc Greneche[4] · Mohamed Khitouni[1]

Received: 10 July 2020 / Accepted: 18 November 2020 / Published online: 3 January 2021

Abstract
Magnetic structures have attracted a great interest due to their multiple applications, from physics to biomedicine. Iron, nickel and cobalt are among the most important ferromagnetic elements, therefore the synthesis of Fe-based alloys processed by ball milling from the Fe, Ni and Co powders is of particular interest. This subject mainly concerned the structural and magnetic properties evolution of $Fe_{50}Co_{25}Ni_{25}$ nanocrystalline powder mixture prepared by mechanical alloying in a high-energy planetary ball mill under argon atmosphere. For extended milling time of 100 h, two nanocrystalline Fe (Co,Ni) (∼87 nm) and fcc-Co-rich (∼47 nm) phases were identified. This phase transformations, dependent on the alloying time, are related to the increase in dislocations and accumulation of stacking faults. Dislocation density of 1.25×10^{15} m^{-2} is estimated after 100 h of milling. The milled FeCoNi alloy displays a soft ferromagnetic behavior with single magnetic domain (Hc ∼ 12.5 Oe and Mr/Ms ∼ 0.007 for 100 h milling). Mössbauer analysis gives three main magnetic components: two different components attributed to metallic Fe species located in bcc and fcc Fe–Co–Ni domains and a magnetic component characterized by larger hyperfine fields and isomer shifts typical of Fe^{3+}, Fe^{2+} species and Fe ions.

Keywords Mechanical alloying · Nanostructure · Fe-based alloys · X-ray diffraction · Magnetic properties · Mössbauer studies

1 Introduction

Nanocrystalline alloys, especially those characterized by their magnetic properties, are constantly being integrated in all scientific fields, particularly in the medical, electronic and field of information technology [1–3]. Mechanical alloying is an efficient method that can produce nanocrystalline alloys [4–6]. As the grain size decreases, and reached a critical size, the grain contains a single domain, which is uniformly magnetized to its saturation magnetization [7]. Iron alloys exhibit remarkable magnetic properties such as permeability, coercivity, saturation magnetization and magnetic field [8]. The addition of Co in iron-based alloys ameliorates the soft magnetic properties in this type of alloys [9]. When the increased of the Ni content on Fe–Co–Ni alloy synthesized by the chemical reduction method leads to a decreasing of the Ms and a reached of higher value of coercivities , These results provide the opportunity for the synthesis of magnetic ternary alloys with tunable magnetic properties [10], wheras. The addition of Ni in Fe exhibited larger coercivity with increasing milling time, whereas the saturation intrinsic flux density was increased at the early stages of milling time and then decreased at longer stages [11]. Thus, by addition of Ni to the Fe–Co alloys, the electrical resistivity and permeability were enhanced [12]. The ternary alloy Co–Fe–Ni demonstrates good soft magnetic properties which can be applicable to design of some devices such as write head core

Electronic supplementary material The online version of this article (https://doi.org/10.1007/s13369-020-05166-2) contains supplementary material, which is available to authorized users.

✉ Rakia Daly
daly.rakia@gmx.fr

1 Laboratoire de Chimie Inorganique, LR 17-Es-07, FSS, Université de Sfax, BP 1171, Sfax, Tunisia

2 Dep. de Fisica, Universitat de Girona, Campus Montilivi, 17071 Girona, Spain

3 Dep. CMEM, Universitat de Barcelona, Marti Franques 1, 08028 Barcelona, Spain

4 Institut des Molécules et Matériaux du Mans, IMMM, UMR CNRS 6283, Université du Maine, Avenue Olivier Messiaen, 72085 Le Mans Cedex 9, France

materials in hard disk [5]. These properties are influenced by structural changes and the formation of internal defects [13]. On the other hand, Fe–Ni alloys were characterized by low coercive fields and high saturation, which are beneficial to use in the industrial field [14]. Fe–Co–Ni alloys that remain stable at high temperature are characterized by magnetic soft properties [15]. These types of alloys are commonly used for the manufacture of magnetic recording ultra-high-density systems with different sensors and diminutive devices as a catalyst [16–18]. Mechanical milling is one of the techniques providing some superior properties of FeCoNi alloy [19, 20]. Currently, several studies are interested in the possibility of synthesis FeCoNi nanoparticles in a carbon matrix of synthesized metal–carbon nanocomposites based on polyacrylonitrile and metal salts [21].

In the present work, we choose to study iron triad nanomaterials $Fe_{50}Co_{25}Ni_{25}$ due to their wide range of application in energy and environment fields [16]. In this case, the studying of the magnetic and microstructural properties evolution notably as a function of milling is very important in order to create new compositions destined for specific applications. The present analysis focuses on the structural and microstructural changes that occurred in Fe, Co and Ni phases during the milling of the Fe–25 at%Co–25 at%Ni powder mixture. The microstructure of the different phases is characterized in terms of crystallite size, lattice strains and dislocation density. To achieve this objective, the relative abundances of the individual phases are determined from the X-ray diffraction profiles (XRD) using the Rietveld refinement [22]. In addition, changes in the magnetic properties of mechanically alloyed powder mixtures are investigated during the milling process.

2 Materials and Experimental Procedures

The mixture of $Fe_{50}Co_{25}Ni_{25}$ (at%) powder was prepared in proportions corresponding to the nominal composition from the elemental powders of Fe (99.97% purity, mean particle size < 10 μm), Co (99.9% purity, mean particle size < 2–5 μm) and Ni (99.7% purity, mean particle size < 10 μm) by using a high-energy planetary ball mill (Type Fritsch Pulverisette 7) under Ar atmosphere. Ball milling experiments were carried out in a hardened steel container. The ball-to-powder weight ratio (Q) is 2:1, and the milling speed (ω) was adjusted to 600 rpm. Different milling times ranging from 0 to 100 h were used. The milling sequence was chosen as follows: 10 min of milling followed by 5 min of inactivity, to prevent the powder from sticking to the container walls and balls, and the agglomeration of the powder during milling.

X-ray diffraction measurements were performed using Siemens D-500 equipment with CuK_α radiation. Crystallite size, lattice strains and lattice parameters were calculated using the Rietveld method with the Maud program [22]. In all refined XRD patterns, refinement parameter R_{exp} is lower than 10.5% and GOF parameter is lower than 1.6. The morphology and the composition of mechanically alloyed powders were examined by scanning electron microscopy (SEM) in a DSM960A ZEISS microscope in secondary electron mode operating at a voltage of 15 kV. The SEM was equipped with a Vega_Tescan energy-dispersive X-ray spectrometry (EDS) analyzer. The magnetic characterization was carried out by Superconducting Quantum Interference Device from Quantum Design SQUID MPMS-XL at 300 K (about 150 mg of powder in each experiment).

In addition, the mixing of precursors at the atomic level was followed by using conventional transmission ^{57}Fe Mössbauer spectrometry at room temperature using a ^{57}Co source diffused into a rhodium matrix. Moreover, the Mössbauer spectra were fitted by means of the Mosfit program [23] involving quadrupolar doublet and magnetic sextets with Lorentzian lines and discrete distribution of magnetic sextets to describe the broadened magnetic components. Then, the values of isomer shift were referred to that of α-Fe at room temperature while the proportions of each Fe species are derived from the relative absorption area of the corresponding component, assuming the same recoilless f-factor.

3 Results and Discussion

3.1 Phases Analyses

Figure 1 shows the XRD patterns of the powder mixture $Fe_{50}Co_{25}Ni_{25}$ before and after milling. The XRD pattern of the un-milled powder mixture indicates the presence of the characteristic peaks of pure bcc-Fe (SG Im-3 m; $a = 2.866$ Å), hcp-Co (SG P63/mmc; $a = 2.500$ Å and $c = 4.140$ Å) and fcc-Ni (SG Fm-3 m; $a = 3.523$ Å). From 2 h milling, one can observe the broadening of the diffraction peaks and the decrease in their intensities with increasing milling time. Among the lattice planes, the peak at ~ 45° for all samples, corresponding to the crystal plane (110), was more intense than the other peaks suggesting that this was the predominant peak representing the preferred orientation (texture) and the size of the crystal domain.

This can be explained by the decrease in crystalline grain size during milling and the existence of internal stresses, which are gradually introduced by high-energy mechanical milling. After 50 h milling, the disappearance of hcp-Co and fcc-Ni peaks may be due to the distribution of these atoms in the Fe lattice resulting in the formation of supersaturated solid solution bcc-Fe(Co,Ni). After 100 h of milling, one can notice the appearance of new diffraction peaks, on the lower angle side of hcp-Co ones, due to the formation of the fcc-Co solid solution. This can be explained by the allotropic trans-

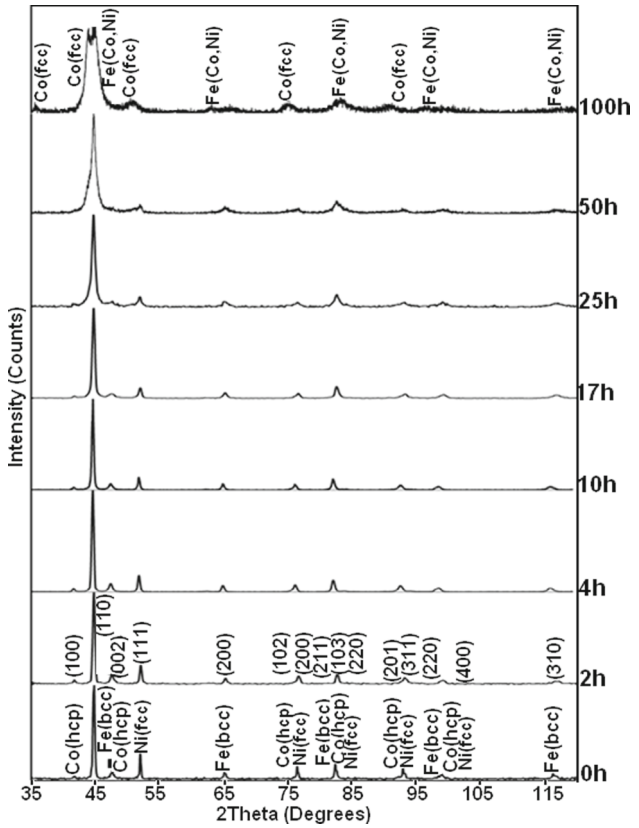

Fig. 1 XRD patterns of $Fe_{50}Co_{25}Ni_{25}$ powders collected at different milling times

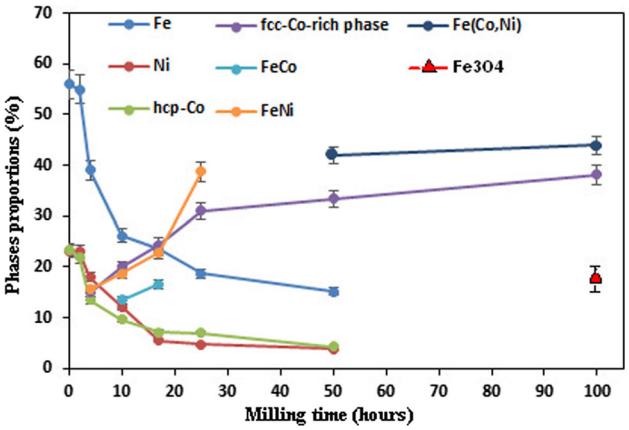

Fig. 2 Evolution of the phases proportions as a function of the milling time

formation of hcp-Co to fcc-Co. Extensive research on the allotropic transformation of Co after ball milling has suggested that the control of the hcp-Co phase is determined by the milling intensity that is related to the ball-powder weight ratio. Indeed, with the present milling condition (Q = 2:1; ω = 600 rpm), the hcp-Co phase becomes unstable when external mechanical energy is introduced. Cardellini and Mazzone [24] reported that after a few hours of milling, one could observe that the hcp-Co phase transforms into a disordered phase composed of close-packed planes arranged in a random sequence. Further, milling does not affect the stability of this phase up to the point where iron contamination induces the transition from hcp-Co to the fcc-Co structure. In other words, this behavior can be explained by the presence of stacking faults resulting from plastic deformation during the high-energy mechanical milling [25, 26]. At the same time, one can see the formation of small content of fine grains of Fe oxide (~18%) associated with the oxygen that reacted with iron when exposed to air after ball milling and then during milling but not detected for lower milling times.

Figure 2 gives the evolution of the phase proportions during the milling process calculated based on Rietveld refined powder X-ray diffractograms of all the milling Times (0 h, 2 h, 4 h, 10 h, 17 h, 25 h, 50 h and 100 h) (Fig S1). There is a monotonous decrease in Fe, hcp-Co and Ni proportions until they disappear completely after 100 h of milling. Further, the proportions of Fe(Co)- and Fe(Ni)-type solid solutions reached maximum values of 16.5% (after 17 h milling) and 38% (after 25 h of milling), respectively.

Also, one can observe the formation of Fe(Co,Ni)-type solid solution with a proportion around 42% (Fig. 3a). On the other hand, the proportion of the fcc-Co-rich phase formed after 4 h milling gradually increases from 15 up to 38% after 100 h. At the same time, one can notice the coexistence of Fe(Co,Ni)-type solid solution and fine Fe_3O_4 oxide with proportions of 44 and 18%, respectively (Fig. 3b). In their recent work, Alleg et al. [27] have related such variations to the complexity of the alloying process through the diffusion of atoms.

Figure 4 shows the changes in microstructural parameters, in terms of the crystallite size (D) (Fig. 4a) and the lattice strains (ε) (Fig. 4b), with milling time. Clearly, the reduction in crystallite size is accompanied by an increase in the lattice strain as the milling time increases. As expected, this is a common behavior for all alloys prepared by MA [27]. As can be seen in Fig. 4a, the 100 h MA powdered product consists of metastable bcc-Fe(Co,Ni) and fcc-Co nanocrystals with crystallite of about 30–40 nm mean sizes. While at the early stages of process the lattice strain increases rapidly with the increasing milling time than beacames slow on longer milling times. At the end of the milling process, it reached final values of 0.98 and 1.28% for final products bcc-Fe(Co,Ni) and fcc-Co, respectively (Fig. 4b). As reported by Koohkan et al. [11], lattice strains in crystalline grains come from various sources such as vacancies, dislocations, shear planes, thermal expansions and contractions. In addition, Chen concluded that the increase in residual strains inside the crystallite could be due to the stress fields associated with the multiplication of the dislocations. On the other hand, as we have reported in previous work [28], the modification of the chemical composition

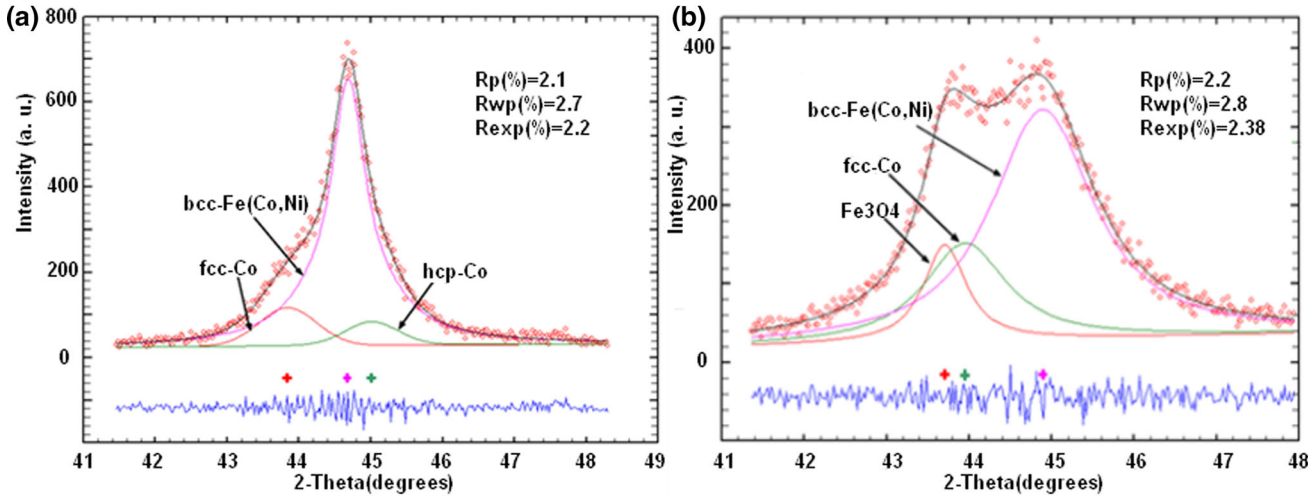

Fig. 3 Observed (points) and calculated (solid line) room temperature X-ray diffraction patterns of (110)Fe peaks for**a** 50 h and **b** 100 h. Positions of the Bragg reflections are represented by vertical bars. The observed calculated difference pattern is depicted at the bottom of each figure

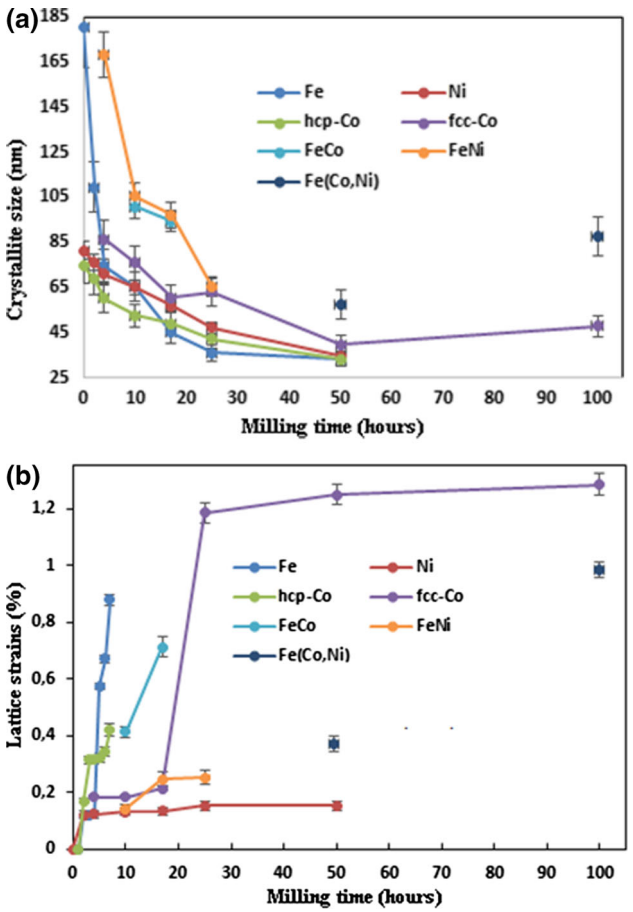

Fig. 4 Evolution of microstructural parameters versus milling time: **a** crystallite size and **b** lattice strains

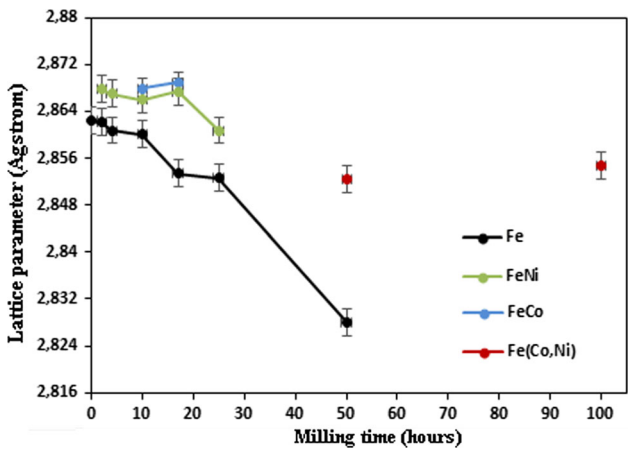

Fig. 5 Lattice parameter variations in Fe, Fe–Ni, Fe–Co and Fe (Co,Ni) against milling time

of the powder mixture at the nanoscale, following the formation of solid insertion or substitution solutions, plays an important role in the variation of microstructural parameters in terms of crystallite size and microstrains.

The lattice parameters calculated for Fe and bcc-Fe-rich metastable nanocrystals as a function of milling time are listed in Fig. 5. The lattice parameter of Fe decreases from 0.2862 nm before milling to 0.2828 nm for 50 h milling.

The values of lattice parameters of metastable bcc-Fe-rich nanocrystals (FeCo, FeNi and Fe (Co,Ni)) are slightly higher than that of the pure bcc-Fe phase during the whole milling process. These high values of lattice parameters can be due to the dissolution of the cobalt and nickel atoms by their insertion or their substitution in the iron network. The supersaturated solid solution Fe(Co,Ni) obtained at the end of the mechanical milling has a lattice parameter of 0.2854 nm. The decrease in lattice parameters may be due to particles compression due to the presence of the compressive fields within the boundaries of non-equilibrium particles inside of

crystallites, and therefore results in a decrease in the lattice parameter [29]. In addition, Suryanarayana [30] reported that this decrease may be due to the allotropic phase transformation of hcp-Co → fcc-Co and/or the triple defect disorder.

For milled samples, dislocations are of paramount importance for the mechanical and physical properties of nanocrystalline materials. Their presence in large quantities in nanocrystalline materials obtained by mechanical milling facilitates the formation of alloys and supersaturated solid solutions at low temperatures by accelerating the diffusion of the atoms. The calculated dislocation densities are around 3.10^{15} m^{-2} and 8.10^{15} m^{-2} for the bcc-Fe(Co,Ni) and fcc-Co nanocrystals, respectively. These values are lower than the dislocation density limit achieved by plastic deformations in metals (10^{16} m^{-2} for corner dislocations). This suggests that the dislocations generated during the present mechanical alloying are of a mixed nature (screw and edge dislocations) [31].

Figure 6 illustrates the morphological shape and the corresponding quantitative analysis of powder particles of the mixture $Fe_{50}Co_{25}Ni_{25}$ before and after various milling times. Before milling, the powder particles have a rounded shape with fine sizes ranging between 8 and 10 μm (Fig. 6a).

The results of the corresponding EDX analysis show the presence of the three elements Fe, Co and Ni (Fig. 7a).

During milling, the powder particles are continuously subjected to the repeated effects of fracture and welding, leading to the formation of aggregates whose particle size is the result from the competition between these two phenomena. The evolution of the morphology of the powders during mechanical milling is related to the difference between the mechanical properties of the elements. After 2 h of milling, Fe and Ni, which are ductile metals, deform strongly plastically with the appearance of flattened particles and flakes as a result of the ball-and-powder and ball-powder-wall collisions by a process of micro-forging (Fig. 6b). However, Co, which is fragile, will rather tend to fracture. The fragments of Co become small enough to promote short-range diffusion, and the brittle elements have some solubility in the ductile matrix. This mixture causes a change in the shape of the individual particles, and as a result, the particles have a small increase in size up to a value of 15 μm. After 4 h of milling, the Co particles gradually integrate the ductile particles of Fe and Ni thus forming solid solutions. During this period, the composite agglomerates obtained, which are about 65 μm larger in size, are not homogeneous in composition (Fig. 6c). Beyond 17 h of milling, the distribution of the particles is non-uniform in the size and shape (Fig. 6d). For milling times longer than 25 h, the powder particles are refined to their minimum average size of about 2 m at the end of the milling process (Fig. 6e, f). The size distribution of the powder particles was estimated from SEM micrographs (Fig. 7d). Three stages were noted as an increase (stage I) followed by a decrease (stage II) and ended with a stationary steady-state (stage III). During the MA process, control of the chemical composition of the elements was necessary due to contamination of the powders on the surface and at the interfaces by the tools and the milling atmosphere. The results of the qualitative analysis of the milled powders for 2 and 25 h show the presence of only the three elements Fe, Co and Ni (Fig. 7a, b), while for 100 h, we can see the presence of small content of oxygen absorbed on the surface of the powder when exposed to air after ball milling. In addition, it is important to note that no additional peaks of impurities and contamination derived from milling tools were observed.

3.2 Magnetic Properties

Figure 8 compares the magnetization curves, measured at 300 K, for the Fe_{50} $Co_{25}Ni_{25}$ mixture powders before and after different milling times. The hysteresis loops reveal a sigmoidal shape as usually observed in magnetically soft nanostructured materials characterized by the presence of small magnetic domains.

As the milling time increases, the variation in magnetic properties can be understood by the effect of the decrease in grain size. Indeed, if the grain size is sufficiently small, other microstructural parameters such as the composition and volume fraction of the individual structural phases can influence the soft magnetic properties [32]. As reported in Fig. 9a, two stages are observed from the variation in the coercive field as a function of the milling time: a slight increase from 69.4 to 77.2 Oe between 2 and 6 h milling, followed by a reduction until reaching a minimum value of 12.5 Oe after 100 h of milling.

The increase in Hc during the initial milling stage can be attributed to the introduction of the defects as well as to dislocations, stacking faults, microstrains, grain boundaries…) [33, 34]. Consequently, the increase in these defects as well as the fact that the grain sizes exceed the domain wall thickness and so the grain boundaries act as impediments to the domain wall motion [34]. In addition, the increase in Hc is consistent with SEM observations showing that the ductile particles of Fe and Ni powders are flattened by compressive forces (Fig. 6b). The elongated shape gives the powder particles a preferred direction of magnetization oriented along their major axis and the shape anisotropy opposes the reversal of the magnetization and increases the coercive field [35]. On the other hand, the reduction in the coercive field for longer grinding times can be correlated with the reduction in grain size and therefore with the deviation of interatomic distances in the interfacial regions relative to the crystalline component. It has been shown that this reduction for a material at a few nm could be attributed to the presence of superparamagnetic particles [32]. The superparamagnetic characteristic of MA Fe-based alloy powders has been con-

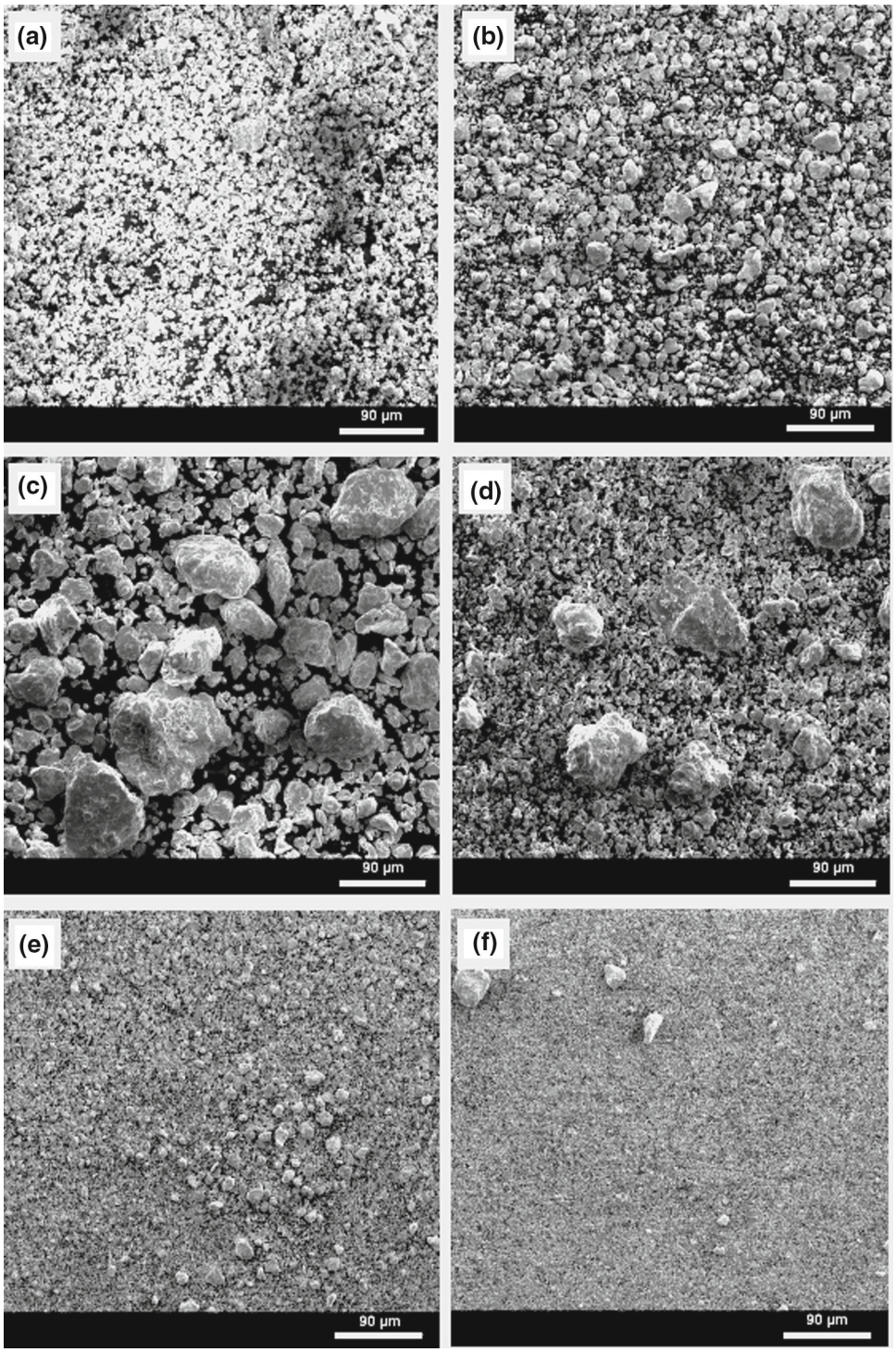

Fig. 6 Morphological evolution of the powder particles of the $Fe_{50}Co_{25}Ni_{25}$ mixture **a** before and after different milling times: **b** 2 h, **c** 4 h, **d** 17 h, **e** 25 h, **f** 100 h

firmed by Mössbauer spectrometry [36]. It has been reported that the superparamagnetic limit for $Fe_{50}Co_{50}$ was reported to be about 34 nm [37], some particles for the present MA powder could be smaller than 34 nm.

The variation in saturation magnetization Ms with milling time is given in Fig. 9b. As can be seen, Ms gradually increases from 104 to 187 emu/g with increasing milling time up to 50 h. After that, we noticed a decrease in the magnetization saturation up to 124 emu/g. The saturation magnetization (Ms) strongly depends on chemical composition and electronic structures, such as charge transfer and spin–orbit coupling [38, 39]. The increase in Ms can be attributed to the alloying and the decrease in magnetocrystalline anisotropy due to the refinement of the microstructure,

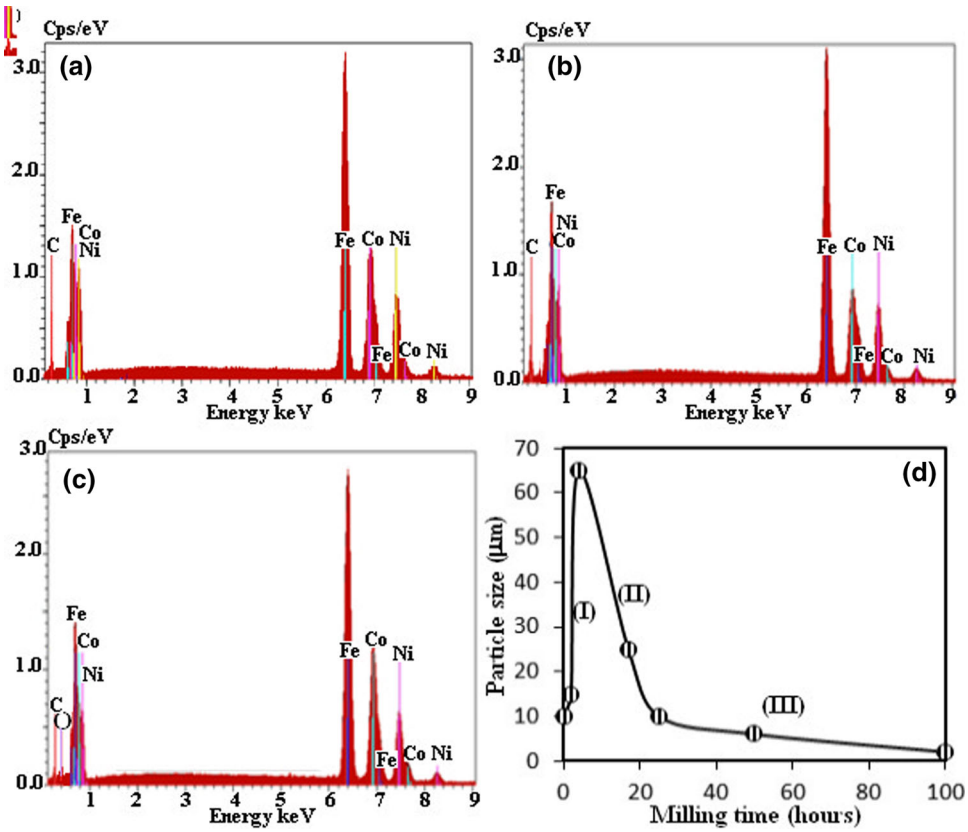

Fig. 7 EDX analysis of powder particles of $Fe_{50}Co_{25}Ni_{25}$ powder after different milling: **a** 2 h, **b** 25 h and **c** 100 h. **d** Variation in the average particle size of powders during mechanical milling

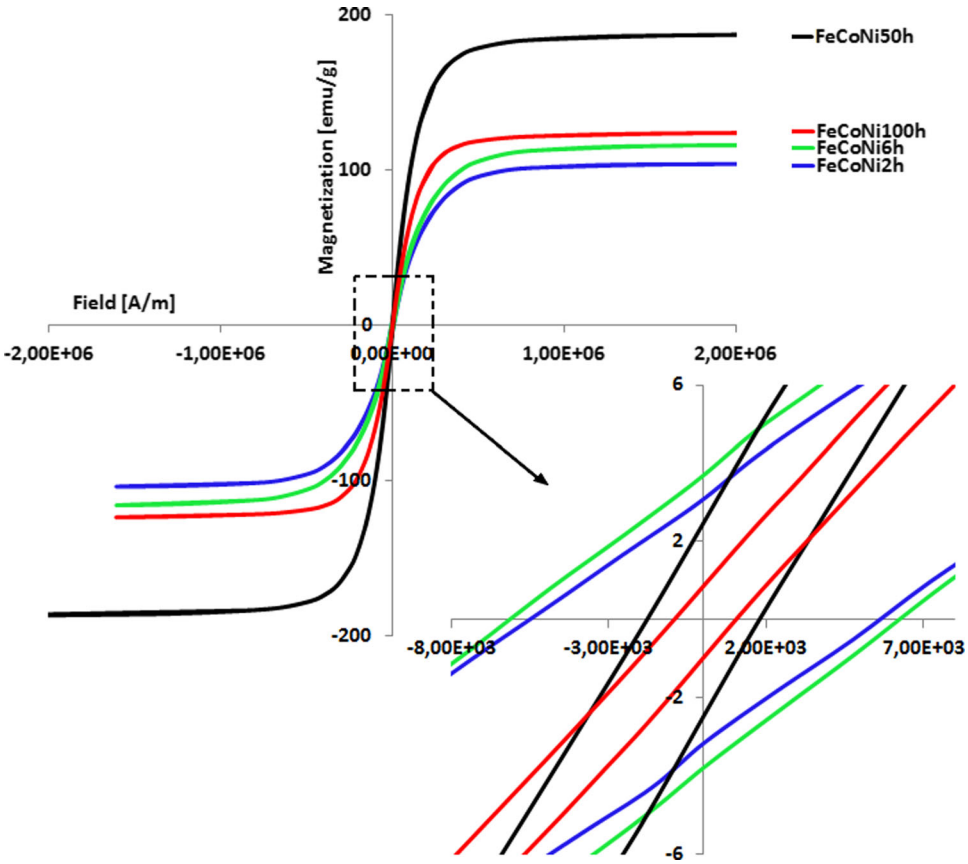

Fig. 8 Typical hysteresis loops dependence on milling time of the mixture $Fe_{50}Co_{25}Ni_{25}$, at $T = 300$ K

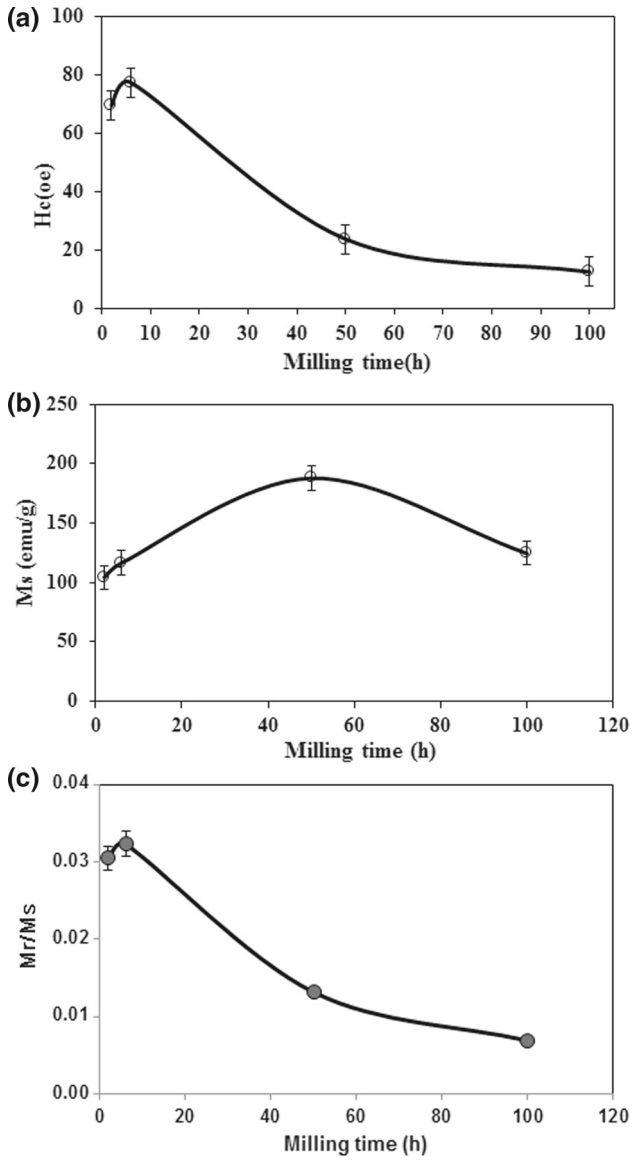

Fig. 9 Coercive field Hc (**a**), saturation magnetization Ms (**b**), and remanence-to-saturation ratio, Mr/Ms (**c**) as a function of milling time of the mixture $Fe_{50}Co_{25}Ni_{25}$

which results in an easier rotation of the magnetic vector. But the decrease in Ms can be related to the decrease in grain size. Indeed, if the grain sizes are small enough, structural distortions associated with surfaces/interfaces reduce the magnitude of saturation magnetization owing to the deviation of the interatomic spacings in the interfacial regions. In addition, this decrease in the Ms value can be related to the modification of magnetization of the elements during milling due to the presence of crystalline defects among these elements, the magnetic alloys which produced a stronger magnetic field than the other elements [39]. The remanence-to-saturation ratio, Mr/Ms, which is an important magnetic parameter in determining the magnetic energy, is plotted against milling time in Fig. 9c. All powder mixtures processed by MA have a ratio (Mr/Ms) between 0.007 and 0.033 which is much lower than that expected for a single-domain particle. This may indicate the possibility that although the particle size is in the nanometer range, magnetic grains still have a multi-domain structure; since, in single-domain particles with uniaxial anisotropy, the reduced remanence is of the order of 0.5 and the coercivity is expected to follow the D^6 law [37] that is not the case in the present study.

3.3 Mössbauer Analysis

To get a complementary description of the structure of the present ball milled powders, transmission ^{57}Fe Mössbauer spectrometry was carried out at 300 and 77 K (Fig. 10a, b). Some spectra are compared in Fig. 10a: They allow to follow the phase transformations in the $Fe_{50}Co_{25}Ni_{25}$ (at%) system as a function of the high-energy ball milling times.

For short milling times (4 h), the magnetic spectrum must be described by means of two magnetic components. The major component is characterized by a hyperfine field value typical of that of bcc-Fe and can therefore be attributed to pure bcc-Fe domains while the minor component is attributed to bcc-Fe domains with the presence of diffused Co and Ni atoms for the mechanical milling. Indeed, it has been shown that changes in the hyperfine field can be due to a core polarization term resulting directly from changes in d-moment at the Fe sites, and a conduction electron polarization (CEP) term resulting from changes induced by the distribution of d-moment on the impurity and at the Fe sites. As a result, the hyperfine field at Fe sites is increased in presence of some Co and Ni impurities.

By increasing the milling time (t >25 h), a significant change in the hyperfine structure is clearly observed with an asymmetric broadening of the magnetic lines and the presence of a central quadrupolar structure. The first description consists, on the one hand, of a magnetic component resulting from a discrete distribution of hyperfine fields, some values of which exceed 33 T, while the others are smaller. As previously concluded, the highest values are due to Fe sites located in Co- and/or Ni-enriched bcc-domains. On the contrary, the smallest values are due to Fe sites located into either Ni or Co fcc-domains. Therefore, we considered two distributions of hyperfine fields leading to two magnetic components attributed to Fe sites located in bcc and fcc Fe–Co–Ni domains. On the other hand, the central quadrupolar feature was described by means of a distribution of quadrupolar splitting. The main information results from the isomer shift, the value of which does not allow to conclude that neither ferric nor ferrous species is present, but a mixture of them. Consequently, Mössbauer spectra were recorded at 77 K to better understand the complexity of the current nanostructured powders (Fig. 10b). The Mössbauer spectrum obtained

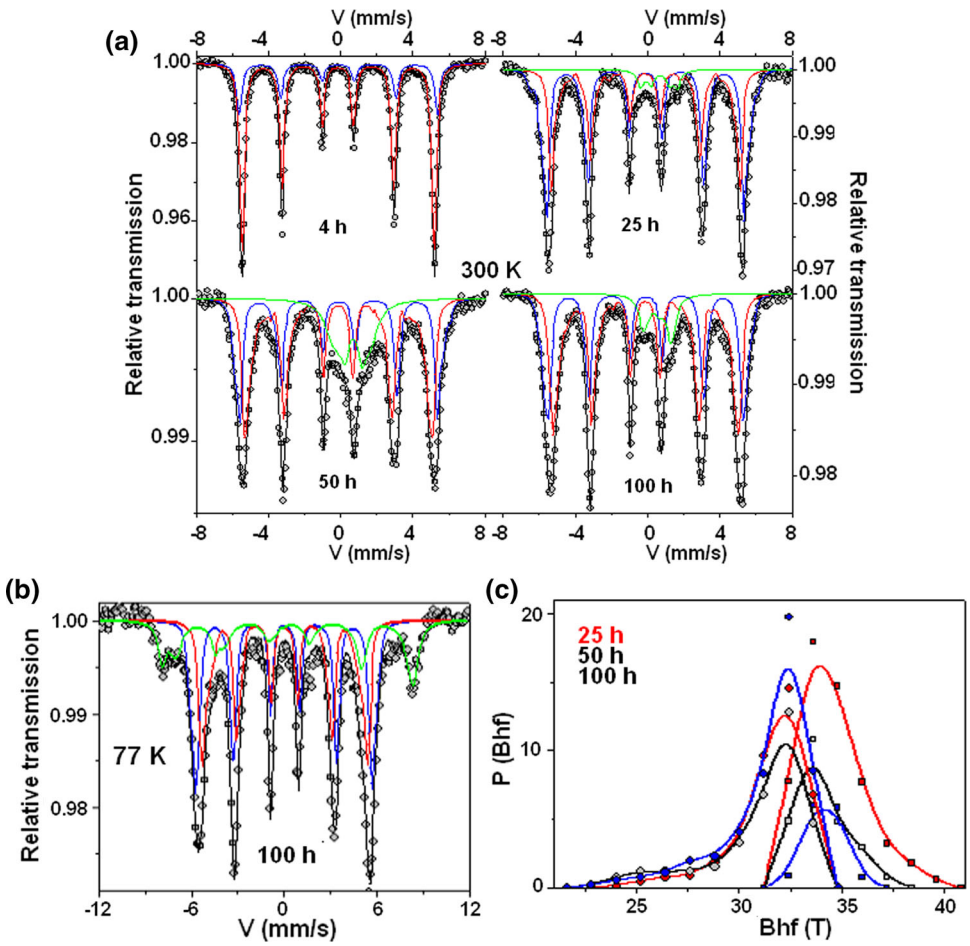

Fig. 10 Room temperature ^{57}Fe Mössbauer spectra of the $Fe_{50}Co_{25}Ni_{25}$ powders milled for 4 h, 25 h, 50 h and 100 h, (**a**) and 77 K ^{57}Fe Mössbauer spectrum of the $Fe_{50}Co_{25}Ni_{25}$ powder milled for 100 h, (**b**) and corresponding hyperfine field distributions (25 h, 50 h, 100 h at 300 K) (**c**)

at 77 K on the powders milled for 100 h shows exclusively magnetic components, as illustrated in Fig. 10b. The fitting model consists of considering three main magnetic components. As is shown in Fig. 10, two different components are clearly attributed to metallic Fe species located in bcc and fcc Fe–Co–Ni domains in agreement with the fitting model used at 300 K. Then, the third magnetic component which is characterized by larger hyperfine fields and isomer shifts typical of Fe^{3+}, Fe^{2+} species and Fe ions with intermediate valency states is attributed to a mixture of magnetite and maghemite phases. It is important to note that this decomposition, which is in agreement with that at 300 K, clearly demonstrates the chemical and structural complexity of the nanostructured powders and is qualitatively consistent with that established from X-ray pattern. Indeed, the nanoscale atomic mixing induced for milling time results from the diffusion of Co and Ni atoms into bcc-Fe grains, that of Fe into fcc-Co and Ni grains, in addition to that of Co atoms into Ni grains and vice versa, leading to a packing of bcc and fcc structural domains containing Fe, Co and Ni metallic species with different proportions and grain boundaries, the chemical composition, the thickness and the proportions remain difficult to estimate.

The remaining question is related to the origin of a significant contribution of Fe oxides observed by Mössbauer spectrometry and probably that of oxides containing Ni and/or Co atoms. For the initial products, oxides were not detected for the elements Fe, Co and Ni for short milling times. However, the problem of oxidation manifests itself for the last milling times as it may be the exposure of the present nanostructured powders to the oxygen from the air, i.e., the precaution by a vacuum followed by an Ar sweep is taken each time, which has been repeated three consecutive times. The powders may also be contaminated with oxygen from the air during storage in the flask, which has not been properly controlled as before milling.

4 Conclusion

Nanostructured $Fe_{50}Co_{25}Ni_{25}$ alloy with soft magnetic properties and with wide range of application in energy field including energy transfer, conversion and storage, and in the environment field, was prepared by mechanical alloying. The most interesting results of this research are as follows:

- Completion of the supersaturated solid solution formation bcc-Fe(Co,Ni) in nanometer scale is accompanied by an allotropic hcp-Co ↔ fcc-Co transformation. This transformation behavior is explained by the type of defects of the network stacks under the effect of high-energy mechanical milling (Fig. 10c). The large density of dislocations (around 10^{15} m^{-2}) in nanocrystalline materials obtained by mechanical milling is considered as responsible for these phase transformations.
- At the macroscopic scale, an increase followed by a decrease in Hc and Ms is observed during milling. This behavior suggests the presence of a non-homogeneous distribution of the Co and Ni atoms around the Fe and consequently a distribution of the magnetic exchange interactions. Hc and Ms parameters strongly depend on chemical composition and electronic structures. Magnetically soft nanostructured materials with single magnetic domains (Mr/Ms ~ 0.007) are obtained at the end of mechanical milling.
- Mössbauer spectrum obtained at 300 K demonstrates two different components clearly attributed to metallic Fe species located in bcc and fcc Fe–Co–Ni domains. Also, the Mössbauer spectrum obtained at 77 K on the powders milled for 100 h shows exclusively magnetic components. Mössbauer measurement demonstrates the chemical and structural complexity of the nanostructured powders which is qualitatively consistent with that established from X-ray pattern.

References

1. Prasad, N.K.; Kumar, V.: Structure–magnetic properties correlation in mechanically alloyed nanocrystalline Fe–Co–Ni–(Mg–Si)x alloy powders. J. Mater. Sci. Mater. Elect. **26**, 10109–10118 (2015). https://doi.org/10.1007/s10854-015-3695-7
2. Raanaei, H.; Eskandari, H.; Mohammad, H.V.: Structural and magnetic properties of nanocrystalline Fe–Co–Ni alloy processed by mechanical alloying. J. Magn. Magn. Mater. **98**, 190–195 (2016). https://doi.org/10.1016/j.jmmm.2015.09.031
3. Siyuan, D.; Tao, N.; Jing, Y.; Hucheng, Y.; Shukui, Z.: Recent advances and applications of magnetic nanomaterials in environmental sample analysis. Trac. Trend. Anal. Chem. **126**, 115864 (2020). https://doi.org/10.1016/j.trac.2020.115864
4. Liming, S.; Yi, Xu: Amorphous behavior of $Zr_xFeNiSi_{0.4}B_{0.6}$ high entropy alloys synthesized by mechanical alloying. J. Non. Cryst. Solids. **530**, 119854 (2020). https://doi.org/10.1016/j.jnoncrysol.2019.119854
5. Pikula, T.; Oleszak, D.; Pękała, M.; Jartych, E.: Structure and some magnetic properties of mechanically synthesized and thermally treated Co–Fe–Ni alloys. J. Magn. Magn. Mater. **320**, 413–420 (2008). https://doi.org/10.1016/j.jmmm.2007.06.020
6. Hiroaki, K.; Hitoshi, M.: Mechanical alloying of Ga_2O_3 and Ga_2O_3-Al_2O_3. Mater. Chem. Phys. **250**, 123080 (2020). https://doi.org/10.1016/j.matchemphys.2020.123080
7. Hapishah, A.N.; Hamidon, M.N.; Syazwan, M.M.; Shafiee, F.N.: Effect of grain size on microstructural and magnetic properties of holmium substituted yttrium iron garnets ($Y_{1.5}Ho_{1.5}Fe_5O_{12}$) mmm Results. Phys. **14**, 102391 (2019). https://doi.org/10.1016/j.rinp.2019.102391
8. Guittoum, A.; Layadi, A.; Bourzami, A.; Tafat, H.; Souami, N.; Boutarfaia, S.; Lacour, D.: X- ray diffraction, microstructure, Mössbauer and magnetization studies of nanostructured $Fe_{50}Ni_{50}$ alloy prepared by mechanical alloying. J. Magn. Magn. Mater. **320**, 1385–1392 (2008). https://doi.org/10.1016/j.jmmm.2007.11.021
9. Inoue, A.; Shen, B.L.; Koshiba, H.; Kato, H.; Yavari, A.R.: Ultra-high strength above 5000 MPa and soft magnetic properties of Co–Fe–Ta–B bulk glassy alloys. Acta Mater. **52**, 1631–1637 (2004). https://doi.org/10.1016/j.actamat.2003.12.008
10. Chokprasombat, K.; Pinitsoontorn, S.; Maensiri, S.: Effect of Ni content on nanocrystalline Fe–Co–Ni ternary alloys synthesized by chemical reduction method. J. Magn. Magn. Mater. **405**, 174–180 (2016). https://doi.org/10.1016/j.jmmm.2015.12.064
11. Koohkan, R.; Sharafi, S.; Shokrollahi, H.; Janghorban, K.: Preparation of nanocrystalline Fe–Ni powders by mechanical alloying used in soft magnetic composites. J. Magn. Magn. Mater. **320**, 1089–1094 (2008). https://doi.org/10.1016/j.jmmm.2007.10.033
12. Jiles, D.: Introduction to Magnetism and Magnetic Materials, pp. 280–297. Chapman & Hall, London (1991)
13. Moumeni, H.; Alleg, S.; Greneche, J.M.: Structural properties of $Fe_{50}Co_{50}$ nanostructured Powder prepared by mechanical alloying. J. Alloy. Compd. **386**, 12–19 (2005). https://doi.org/10.1016/j.jallcom.2004.05.017
14. Msellak, K.; Chopart, J.P.; Jbara, O.; Aaboubi, O.; Amblard, J.: Magnetic field effects on Ni–Fe alloys codeposition. J. Magn. Magn. Mater. **281**, 295–304 (2004). https://doi.org/10.1016/j.jmmm.2004.04.118
15. El-Gendy, A.A.; Ibrahim, E.M.M.; Khavrus, V.O.; Krupskaya, Y.; Hampel, S.; Leonhardt, A.; Büchner, B.; Klingeler, R.: The synthesis of carbon coated Fe, Co and Ni nanoparticles and an examination of their magnetic properties. Carbon **47**, 2821–2828 (2009). https://doi.org/10.1016/j.carbon.2009.06.025
16. Bai, A.; Hu, C.C.; Wen, T.C.: Composition control of ternary FeCoNi deposits using cyclic voltammetry. Electrochim. Acta **48**, 2425–2434 (2003). https://doi.org/10.1016/S0013-4686(03)00266-4
17. Hisada, D.; Fujiwara, Y.; Sato, H.; Jimbo, M.; Kobayashi, T.; Hata, K.: Structure and magnetic properties of FeCo nanoparticles encapsulated in carbon nanotubes grown by microwave plasma enhanced chemical vapordeposition. J. Magn. Magn. Mater. **323**, 3184–3188 (2011). https://doi.org/10.1016/j.jmmm.2011.06.029
18. Mizutani, S.; Yokoshima, T.; Nam, H.S.; Nakanishi, T.; Osaka, T.; Yamazaki, Y.: High-frequency permeability and thermal stability of electrodeposited high-Bs CoNiFe thin films. IEEE. T. Magn. **36**, 2539–2541 (2000). https://doi.org/10.1109/20.908499
19. Loginov, P.; Sidorenko, D.; Bychkova, M.; Petrzhik, M.; Levashov, M.: Mechanical alloying as an effective way to achieve superior properties of Fe–Co–Ni binder alloy. Metals **7**, 570 (2017). https://doi.org/10.3390/met7120570
20. Rathi, A.; Meka, V.M.; Jayaraman, T.V.: Synthesis of nanocrystalline equiatomic nickel-cobalt-iron alloy powders by mechanical alloying and their structural and magnetic characterization. J. Magn. Magn. Mater. **469**, 467–482 (2019). https://doi.org/10.1016/j.jmmm.2018.09.002
21. Muratov, D.G.; Kozhitov, L.V.; Karpenkov, D.Y.; Yakushko, E.V.; Korovin, E.Yu.; Vasil'ev, A.V.; Popkova, A.V.; Kazaryan, T.M.; Shadrinov, A.V. : Synthesis and magnetic properties of Fe—Co–Ni/C nanocomposites. Russ. Phys. J. **60**, 1924–1930 (2018). https://doi.org/10.1007/s11182-018-1304-y
22. Lutterotti, L.: MAUD CPD Newsletter (IUCr). 24 (2000)
23. Varret, F.; Teillet, J.: Unpublished Mosfit Program, Université du Maine France (1976)

24. Cardellini, F.; Mazzone, G.: Thermal and structural study of the h.c.p.-to-f.c.c. transformation in cobalt. Philos. Mag. **67A**(6), 1289–1300 (1993). https://doi.org/10.1080/01418619308225355
25. Sort, J.; Nogués, J.; Suriñach, S.; Muñoz, J.S.; Baró, M.D.: Correlation between stacking fault formation, allotropic phase transformations and magnetic properties of ball-milled cobalt. Mater. Sci. Eng., A **A375–377**, 869–873 (2004). https://doi.org/10.1016/j.msea.2003.10.186
26. Shokrallahi, H.: The magnetic and structural properties of the most important alloys of iron produced by mechanical alloying. Mater. Des. **30**, 3374–3387 (2009). https://doi.org/10.1016/j.matdes.2009.03.035
27. Alleg, S.; Kartoutb, S.; Ibrir, M.; Azzaza, S.; Fenineche, N.E.; Sunol, J.J.: Magnetic, structural and thermal properties of the Finemet-type powders prepared by mechanical alloying. J. Phys. Chem. Sol. **74**, 550–557 (2013). https://doi.org/10.1016/j.jpcs.2012.12.002
28. Lachheb, R.; Bachaga, T.; Khitouni, M.; Makhlouf, T.: Phase transformations and microstructural properties of nanocrystalline $Fe_{75}Si_{10}B_{10}Nb_5$ alloy synthesized by mechanical alloying. Adv. Powder Technol. **26**(6), 1563–1569 (2015). https://doi.org/10.1016/j.apt.2015.08.010
29. Mhadhbi, M.; Khitouni, M.; Azabou, M.; Kolsi, A.: Characterization of Al and Fe nanosized powders synthesized by high-energy mechanical milling. Mater. Charact. **59**, 944–950 (2008). https://doi.org/10.1016/j.matchar.2007.08.001
30. Suryanarayana, C.: Mechanical alloying and milling. Prog. Mater Sci. **46**, 1–184 (2001). https://doi.org/10.1016/S0079-6425(99)00010-9
31. Fecht, H.J.: Nanostructure formation by mechanical attrition. Nanostruct. Mater. **6**, 33–42 (1995). https://doi.org/10.1016/0965-9773(95)00027-5
32. Herzer, G.; in: K.H.J. Buschow (Ed.), *Handbook of Magnetic Materials*, Elsevier Science B.V., 10 (1997)
33. DelshadChermahini, M.; Sharafi, S.; Shokrollahi, H.; Zandrahimi, M.; Shafyei, A.: The evolution of heating rate on the microstructural and magnetic properties of milled nanostructured $Fe_{1-x}Co_x$ (x = 0.2, 0.3, 0.4, 0.5 and 0.7) powder. J. Alloys. Compds. **484**, 54–58 (2009). https://doi.org/10.1016/j.jallcom.2009.05.055
34. Souilaha, S.; Alleg, S.; Djebbaria, C.; Bensalema, R.; Sunol, J.J.: Magnetic and microstructural properties of the mechanically alloyed $Fe_{57}Co_{21}Nb_7B_{15}$ powder mixture. Mater. Chem. Phys. **132**, 766–772 (2012). https://doi.org/10.1016/j.matchemphys.2011.12.010
35. Zeng, Q.; Baker, I.; Mc Creary, V.; Yan, Z.C.: Soft ferromagnetism in nanostructured mechanical alloying FeCo based powders. J. Magn. Magn. Mater. **318**, 28 (2007). https://doi.org/10.1016/j.jmmm.2007.04.037
36. Luborsky, F.E.: Development of elongated particle magnets. J. Appl. Phys. **32**, 171 (1961). https://doi.org/10.1063/1.2000392
37. Kneller, E.; Fine particle theory. In: A.E. Berkowitz, E. Kneller (Eds.), *Magnetism and Metallurgy*, Academic Press, New York. 1. 365–471(1969)
38. Abdellaoui, M.; Djega-Mariadassou, C.; Gaffet, E.: Structural study of Fe–Si nanostructured materials. J. Alloys. Compds. **259**, 241 (1997). https://doi.org/10.1016/S0925-8388(97)00102-3
39. Bensebaa, N.; Loudjani, N.; Alleg, S.; Dekhil, L.; Suñol, J.J.; Sae, M.Al.; Bououdina, M.: XRD analysis and magnetic properties of nanocrystalline $Ni_{20}Co_{80}$ alloys. J. Magn. Magn. Mater. **349**, 51–56 (2014). https://doi.org/10.1016/j.jmmm.2013.08.045